

ARTICLE OPEN



Reduction of lymphotoxin beta receptor induces cellular senescence via the MDMX-p53 pathway

So Young Kim (1)^{1,2}, Bin Lee^{1,3}, Je-Jung Lee^{1,3}, Man Sup Kwak^{1,3}, Woo Joong Rhee (1)^{1,3}, In Ho Park (1)^{3,4} and Jeon-Soo Shin (1)^{1,2,3 ⋈}

© The Author(s) 2025

The lymphotoxin β receptor (LTβR), a key activator of non-canonical NF-κB signaling, is expressed in various cells, including cancer cells. Although high expression of LTBR has been associated with poor patient prognosis and drug resistance, conflicting evidence suggested that LTBR induces apoptosis. To investigate the functional role of LTBR in tumors, we performed LTBR knockdown in cancer cells. We found that LTBR knockdown induced senescence phenomena such as reduced cell number; increased cell size; increased SA-β-Gal activity; and upregulated p53, MDM2 and p21 expression. Moreover, LTβR knockdown induced p21-mediated senescence in p53 WT cancer cells, but not in p53 mutant cancer cells. The level of p53 is regulated by MDM2 and MDMX; MDMX enhances MDM2 activity but is also subject to MDM2-mediated degradation in the nucleus. We found that the intracellular domain of LTβR bound to MDMX thereby inhibited its nuclear translocation, which in turn reduced MDMX ubiquitination and consequently promoted p53 ubiquitination. Additionally, tumors derived from B16F10^{LTβR-KO} cells in WT mice exhibited significantly reduced growth compared to those derived from B16F10WT cells. These results demonstrate that LTBR regulates p53 protein levels by modulating MDMX stability and localization, resulting in p53-mediated cellular senescence.

Cell Death Discovery (2025)11:416; https://doi.org/10.1038/s41420-025-02708-1

INTRODUCTION

The lymphotoxin beta receptor (LTβR), also known as tumor necrosis factor receptor superfamily member 3 (TNFRSF3), is a well-studied molecule in immunology [1-6]. Studies on mice deficient in LTBR have exhibited significant defects in the development and formation of secondary lymphoid organs, including lymph nodes [7]. As a receptor protein, LTBR induces non-canonical NF-κB signaling [8–10]. Upon stimulation and internalization, LTBR recruits TRAF2 and TRAF3, which are subsequently degraded by cIAP1/2. This leads to the cleavage of the p100 precursor bound to RelB, forming the RelB-p52 heterodimer. Furthermore, this signaling is implicated in apoptosis through the LTBR-TRAF2-cIAP1-Smac signaling pathway [11] and cIAP1/2–IKKα/β-mediated canonical NF-κB signaling [12].

Although LTBR signaling activation is known to induce apoptosis [10, 11, 13, 14], some studies have shown a reduced apoptosis rate [15, 16]. Moreover, elevated LTBR expression in several cancer types has been associated with poor patient prognosis [17-20]. These findings suggest LTBR contributes to cancer development and progression, as transfection with truncated or full-length LTBR can result in carcinogenesis [21]. In addition, data from the Cancer Therapeutics Response Portal (CTRP) database of the Broad Institute indicate that LTBR expression is negatively correlated with the efficacy of certain anti-cancer drugs, including doxorubicin (topoisomerase II inhibitor) and nutlin-3a (MDM2 inhibitor). Given the lack of clear mechanism explaining how LTBR affects drug resistance and apoptosis, we aimed to elucidate this gap using an LTBR knockdown system in melanoma cells, where high LTBR expression is correlated with poor survival rate.

The p53 protein is a prominent tumor suppressor and transcription factor [22]. Its expression is induced in response to DNA damage, triggering the expression of various downstream proteins, including MDM2. In turn, MDM2 is a ubiquitin E3 ligase that regulates p53 turnover [23]. Under normal conditions, p53 is maintained at low levels by MDM2. Additionally, MDM2 collaborates with MDMX, a structurally similar protein that lacks E3 ligase activity, to suppress p53. MDMX relies on MDM2 for nuclear localization owing to the lack of nuclear localization signal. MDM2 binds to the MDMX RING domain to facilitate its nuclear import [24]. Following DNA damage, MDMX is translocated to the nucleus by MDM2, where it undergoes degradation, leading to an upregulation of p53. Inhibiting MDMX nuclear translocation results in MDMX accumulation and subsequently leads to the downregulation of p53, MDM2, and p21 [25]. These findings highlight the importance of MDMX localization in regulating p53 degradation. However, how MDMX is stabilized in the cytoplasm remains unclear.

The p53 protein is a key regulator of p21 expression, a cyclindependent kinase (cdk) inhibitor that induces G1/S cell cycle arrest and contributes to cellular senescence [26, 27]. Cellular senescence can be induced by various cellular stress stimuli, such as DNA damage, reactive oxygen species (ROS), and oncogene activation [28]. Senescent cells exhibit distinct morphological

¹Department of Microbiology, Yonsei University College of Medicine, Seoul, South Korea. ²Brain Korea 21 FOUR Project for Medical Science, Yonsei University College of Medicine, Seoul, South Korea. ³Institute for Immunology and Immunological Diseases, Yonsei University College of Medicine, Seoul, South Korea. ⁴Department of Biomedical Sciences, Yonsei University College of Medicine, Seoul, South Korea. [™]email: jsshin6203@yuhs.ac

Received: 6 June 2025 Revised: 22 July 2025 Accepted: 12 August 2025 Published online: 29 August 2025

changes, including increased cell size, a flattened shape, elevated senescence-associated β -Galactosidase (SA- β -Gal) activity, and higher levels of proteins such as p21 [29–31]. Induction of cellular senescence can be used as a promising strategy in cancer therapy, particularly for halting the growth of cancer cells resistant to apoptosis [32, 33].

In this study, we found that LTBR knockdown induces senescence in cancer cells, which is mediated by the upregulation of p53 and p21 expression. We propose that LTBR regulates p53 activity by preventing MDMX nuclear translocation and degradation. These findings provide new insights into the potential of LTBR as a therapeutic target in cancer.

RESULTS

Knockdown of LTBR induces cellular senescence

While the role of LTβR as a receptor is well-documented, recent studies have linked high LTβR expression with poor prognosis in various cancers [20], suggesting its critical role in key cellular processes. To investigate the impact of LTβR knockdown on cellular phenotype, we used specific siRNAs to knock down LTβR expression for 48 h in A375, A549, B16F10, and J774 cell lines (Fig. S1A). LTβR knockdown led to increased cell size and a reduced cell number (Fig. S1B, C). Immunofluorescence staining revealed decreased expression of Ki67, a proliferation marker, in LTβR knockdown cells (Fig. S1D). Further analysis showed an increased proportion of cells in the G1 phase and elevated SA-β-Gal activity, which was detected using the senescence green probe (Fig. S1E, F). Together, these results suggest that LTβR knockdown may induce cellular senescence, which is characterized by growth arrest and apparent morphological changes.

Depletion of LTBR induces p53-mediated senescence

Among the many pathways that drive cellular senescence, we focused on exploring the well-established p53-mediated senescence pathway. To confirm whether the senescent phenotype observed in LTBR knockdown cells is related to p53-mediated pathways, we used doxorubicin (Dox), a well-known inducer of senescence, as a positive control. While Dox-treated cells exhibited reduced cell numbers and increased SA-β-Gal activity, LTβR knockdown in A375 cells similarly led to decreased cell numbers and elevated SA-β-Gal activity, which showed an additive effect when combined with Dox treatment (Fig. 1A, B). To rule out transient effects of siRNA, we prepared LTβR knockout (KO) B16F10 (B16F10^{LTβR-KO}) cells using the CRISPR/Cas9 system. Comparable results were also observed in B16F10^{LTβR-KO} cells (Fig. 1C, D), suggesting that the LTβR depletion induces senescence. Given that p53 is a pivotal regulator of cellular senescence, p53 protein levels were examined (Fig. 1E, F). We observed increased levels of p53, along with elevated levels of MDM2, a key regulator of p53 that is also known to be upregulated during p53-mediated senescence rather than apoptosis [34, 35]. Moreover, we observed an upregulation of p21, a key mediator of p53-mediated cell cycle arrest, in LTβR-depleted cells.

These phenomena were consistent in normal human lung fibroblast IMR90 cells (Fig. S2A–C). However, in the p53 mutant human colorectal cancer cell line HT-29, which lacks p53 transcription activity, senescence was induced by Dox but not by LT β R knockdown, underscoring the role of p53 in LT β R depletion-induced senescence. (Fig. S2D–F). These findings suggest that LT β R regulates cellular senescence through a p53-dependent pathway.

LTBR overexpression attenuates senescence

Next, to investigate the effects of LT β R overexpression on cellular senescence and p53 activity, A375 and B16F10 cells were transfected with either an empty vector plasmid or an LT β R-

expressing plasmid, followed by treatment with Dox. LTβR-overexpressing cells showed a less pronounced reduction in cell number and increase in SA-β-Gal activity compared to control cells when treated with Dox (Fig. 2A–D). Furthermore, western blot analysis revealed lower levels of p53, MDM2, and p21 in LTβR-overexpressing cells compared to controls (Fig. S3A), suggesting that LTβR overexpression reduces Dox-induced senescence in a p53-dependent manner (Fig. 2E, F). To further validate the effect of LTβR overexpression in cells, we restored LTβR expression in LTβR KO cells by transfecting them with an LTβR-expressing vector (Fig. S3B–D). Restored LTβR expression attenuated the senescent phenotype, as shown by increased cell numbers, decreased SA-β-Gal activity, and reduced levels of p53, p21, and MDM2 under Dox treatment. These results indicate that LTβR overexpression can suppress Dox-induced senescence.

LTBR modulates p53 by regulating MDMX protein degradation

To determine whether LTBR influences p53 transcription, p53 transcription levels in LTBR knockdown and overexpressing cells were analyzed using real-time PCR. No significant changes were observed in p53 mRNA levels (Fig. 3A). However, p21 mRNA, a downstream target of p53, was significantly upregulated, suggesting post-transcriptional regulation of p53 by LTBR (Fig. S4A). These results align with previous RNA-seq data showing increased cdkn1a (p21) levels in hematopoietic stem cells of LTBR KO mice [36] (Fig. S4B). Treatment with the proteasome inhibitor MG-132 further elevated p53 levels in LTβR knockdown cells and restored p53 and p21 levels in LTβR-overexpressing cells (Fig. 3B, C). This indicates that knockdown of LTBR prevents degradation of the p53 protein. As p53 protein degradation is regulated by MDM2 and MDMX, we assessed their expression in LTBR knockdown cells. MDMX protein level declined at 12 h after LTBR siRNA transfection, while no significant changes were observed in the level of p53, MDM2, and p21 compared to control cells before 24 h (Fig. 3D and S4C). These findings indicate that the expression of p53, MDM2, and p21 may be influenced as a consequence of changes in MDMX. Knockdown of MDMX increased p53, MDM2, and p21 levels without affecting LTBR expression (Fig. S4D), suggesting that LTBR regulates MDMX, which in turn inhibits p53 degradation. To further support the role of LTBR in p53 protein degradation, A375 cells were treated with MDM2 inhibitor nutlin-3a, which disrupts the MDM2-p53 binding and induces p53-mediated cellular senescence. MDMX overexpression has been reported to counteract the effect of nutlin-3a by preventing p53 activation [37, 38]. In LTβR knockdown cells, p53 levels increased rapidly upon nutlin-3a treatment (Fig. S4E), whereas LTBR-overexpressing cells exhibited a delayed increase (Fig. S4F).

To examine whether LTβR regulates MDMX protein degradation, A375 cells were treated with the protein synthesis inhibitor cycloheximide (CHX). MDMX protein levels decreased more rapidly in LTβR knockdown cells and more slowly in LTβR-overexpressing cells (Fig. 3E, F), indicating that LTβR stabilizes MDMX protein. Finally, changes in MDMX and p53 ubiquitination patterns were observed in both LTβR knockdown and LTβR-overexpressing cells (Fig. 3G–J). Ubiquitination of MDMX was increased in LTβR knockdown cells and decreased in LTβR-overexpressing cells, whereas p53 ubiquitination showed the opposite pattern—decreased in LTβR knockdown cells and increased in LTβR-overexpressing cells. These results suggest that LTβR negatively regulates MDMX ubiquitination, thereby promoting p53 degradation.

LTBR interacts with MDMX in cytosol

We hypothesized that LT β R stabilizes the MDMX protein by binding to it, as LT β R contains an α -helix near its intracellular TRAF-binding domain and MDMX has a Zn²⁺ finger-like domain in its MDM2-binding region. To assess the potential interaction, we



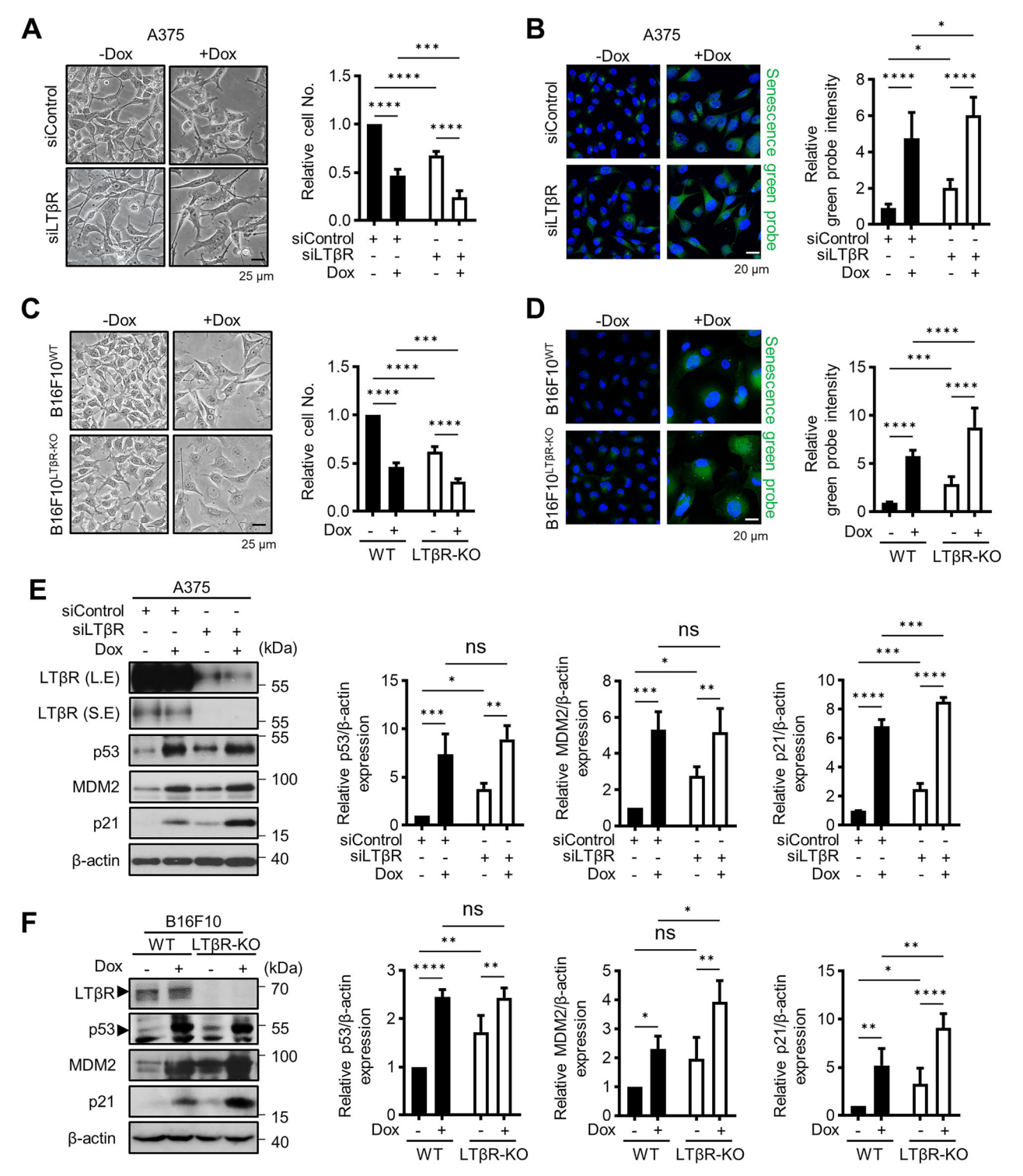


Fig. 1 Depletion of LTβR induces p53-mediated senescence. A, B A375 cells were transfected with 100 nM of siControl (control siRNA) or siLTβR (LTβR siRNA), followed by 100 ng/ml Dox treatment for 48 h. Morphological changes, relative cell number (**A**), and confocal images of a senescence green probe (**B**) were analyzed. **C**, **D** B16F10^{WT} (LTβR WT), and B16F10^{LTβR-KO} (LTβR knockout) cells were treated with 100 ng/ml Dox for 48 h. Morphological changes and relative cell number (**C**), and confocal images of senescence green probe (**D**) were examined. **E**, **F** Western blot images of A375 and B16F10 cells showing the indicated proteins in LTβR-depleted cells. S.E. short exposure, L.E. long exposure. Band intensities of p53, p21 and MDM2 were measured using ImageJ and normalized to β-actin. Results are presented as the mean ± SD from three separate experiments. **B**, **D** Fluorescence intensities for relative senescence green probe were quantified by ImageJ, and data are shown as mean ± SD from three independent experiments (n = 3). *p < 0.05, **p < 0.001, ****p < 0.0001, ****p < 0.0001, using Fisher's LSD post hoc test. n.s not significant.

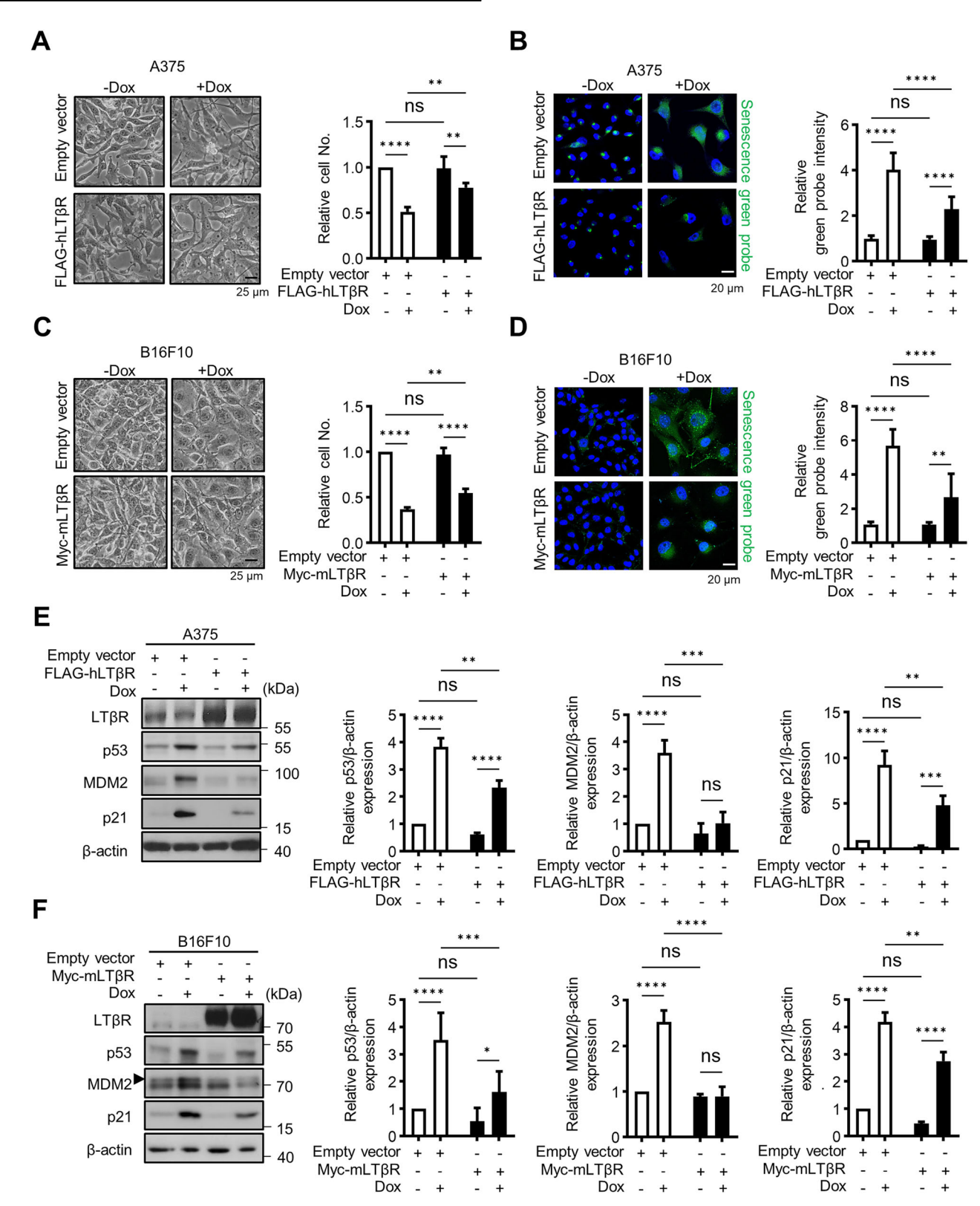
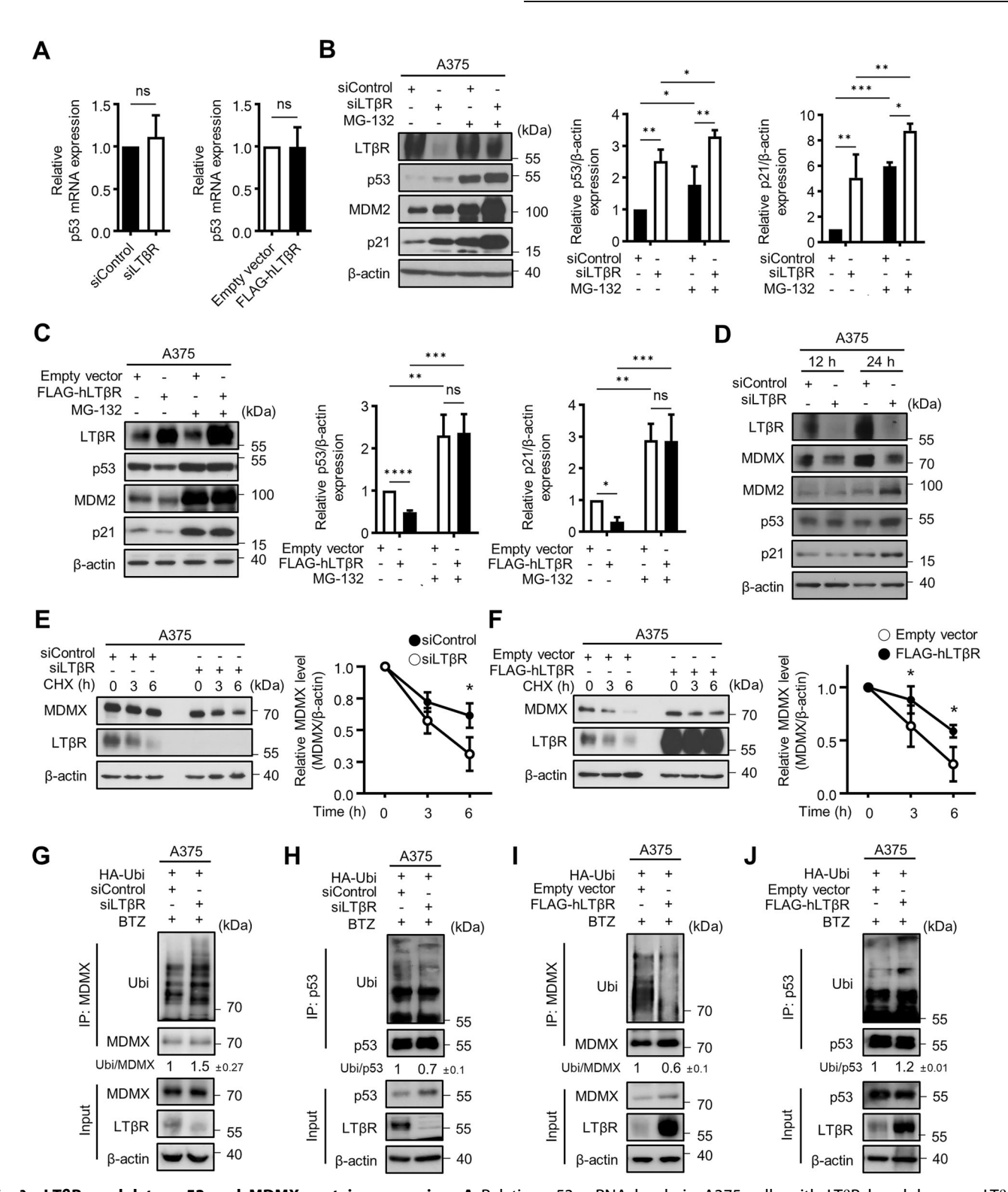


Fig. 2 LTβR inhibits senescence. A–D A375 and B16F10 cells were transfected with LTβR plasmid followed by 100 ng/ml Dox treatment for 48 h. Cells were photographed for analyzing morphological change and relative cell number (**A**, **C**), and stained using a senescence green probe (**B, D**). Relative fluorescence intensity for the senescence green probe was quantified using ImageJ. **E, F** Western blot images of A375 and B16F10 cells for the indicated proteins are representative of three experiments, and the relative p53, p21, and MDM2 protein levels were measured. Bands were quantified using ImageJ software and normalized to β -actin. Graphical data are represented as mean \pm SD from three independent experiments (n = 3). *p < 0.05, **p < 0.01, ****p < 0.001, ****p < 0.0001, using Fisher's LSD post hoc test. n.s, not significant.

4



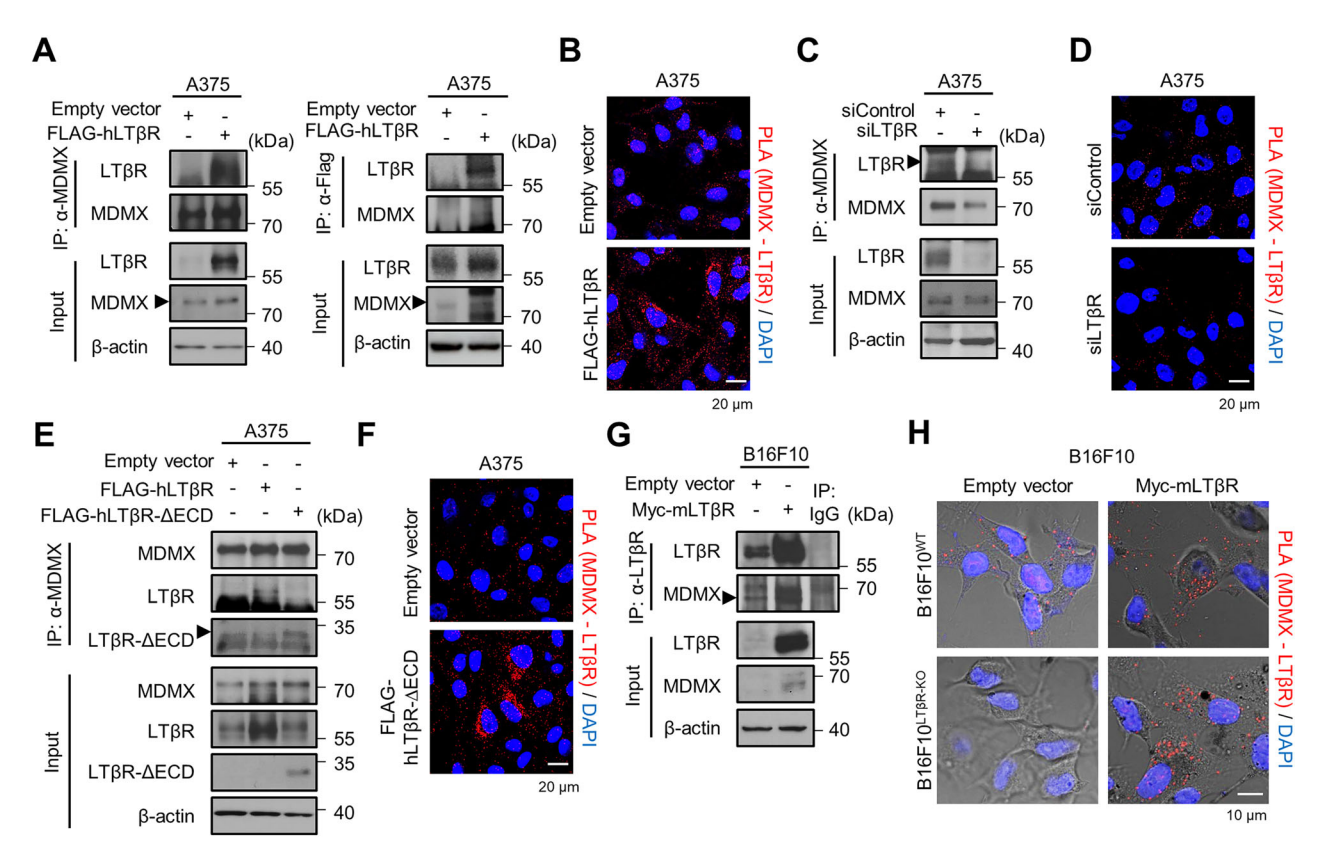


Fig. 4 LTβR interacts with MDMX in the cytosol. A, B A375 cells were transfected with LTβR plasmid for 48 h. LTβR-overexpressing cells were subjected to immunoprecipitation with LTβR and MDMX, and PLA was performed using MDMX, Flag, and LTβR antibodies. **C, D** A375 cells were transfected with 100 nM of siControl or siLTβR for 48 h, and subjected to immunoprecipitation and PLA using LTβR and MDMX antibodies. **E, F** Immunoprecipitation and PLA of extracellular domain (ECD)-deleted LTβR-transfected cells were performed using MDMX and LTβR antibodies. **G** Immunoprecipitation of LTβR and immunoblotting using MDMX antibody validated the interaction in LTβR-overexpressing B16F10 cells. **H** B16F10^{WT} and B16F10^{LTβR-KO} cells were transfected with LTβR plasmid, and PLA was performed to determine the location of interaction between LTβR and MDMX.

used the HADDOCK 2.4 web server to predict the protein-protein docking score. The computational analysis of HADDOCK score for LTBR α -helix-MDMX-MDM2 binding site was -66.1 ± 2.2 (cluster size 21, Z score -1.3), suggesting high probability of binding [39, 40]. To confirm the interaction between LTBR and MDMX, LTBR knockdown and overexpressing cells were subjected to immunoprecipitation and proximity ligation assays (PLA). LTBRoverexpressing cells showed increased LTBR-MDMX binding, whereas LTBR knockdown cells exhibited reduced interaction (Fig. 4A–D), supporting an interaction between LTβR and MDMX. To test whether this binding occurs through the intracellular domain, we generated a truncated form of LTβR (ΔΕCD; Δ1-227 aa), which lacks the extracellular domain but retains the transmembrane and intracellular regions. Both immunoprecipitation and PLA demonstrated that LTBR-ΔECD still interacts with MDMX, suggesting that the interaction occurs in the cytoplasm (Fig. 4E, F). We also observed increased interaction in LTβRoverexpressing B16F10 cells, as well as restored PLA signal in LTβR-overexpressing B16F10^{LTβR-KO} cells (Fig. 4G, H), confirming that this interaction also occurs in mouse cells.

It has been shown that overexpression of LT β R activates non-canonical NF- κ B signaling through self-oligomerization, independent of its extracellular domain [41–44]. To investigate whether the extracellular domain is required to attenuate cellular senescence, we transfected A375 cells with LT β R- Δ ECD, a truncated form lacking the extracellular domain. The results were consistent with those of full-form LT β R overexpression, indicating that the effects are independent of extracellular domain (Fig. S5A–C).

Next, A375 cells were treated with LIGHT protein (a LTBR ligand) (Fig. S6A-D) to examine whether extracellular signaling contributes to p53-mediated cellular senescence. LIGHT treatment resulted in increased levels of IκBα and decreased levels of LTβR, consistent with previous research showing that ligand-induced endocytosis of LTβR limits canonical NF-κB signaling and promotes its degradation [44]. Although LIGHT treatment reduced LTBR expression, MDMX protein levels remained unaffected, which is likely due to decreased levels of MDM2, a MDMXdegrading enzyme. We observed decreased levels of p53 and MDM2 in LIGHT-treated cells, suggesting that p53 and MDM2 levels might be regulated through LTβR-dependent NF-κB signaling. LIGHT treatment led to a comparable increase in p21 levels in both control and LTβR-overexpressing cells, in contrast to the results observed in our overexpression model. The SA-B-Gal activity assay further suggests that LIGHT does not significantly affect the senescence state in LTBR knockdown cells, but induces minor changes in LTBR-overexpressing cells (Fig. S6B, D). To examine whether LIGHT treatment affects the interaction between LTBR and MDMX, we treated cells with LIGHT for 4 h (Fig. S6E). However, the interaction appeared to be primarily regulated by the expression levels of LTBR following LIGHT treatment. Taken together, p53, MDM2, and p21 may be influenced by NF-κB signaling, while MDMX-p53-mediated cellular senescence is likely associated with the expression of LTβR.

LTBR inhibits MDMX nuclear translocation

MDMX lacks a nuclear localization signal and is known to be ubiquitinated in the nucleus by MDM2 [25, 45]. To investigate

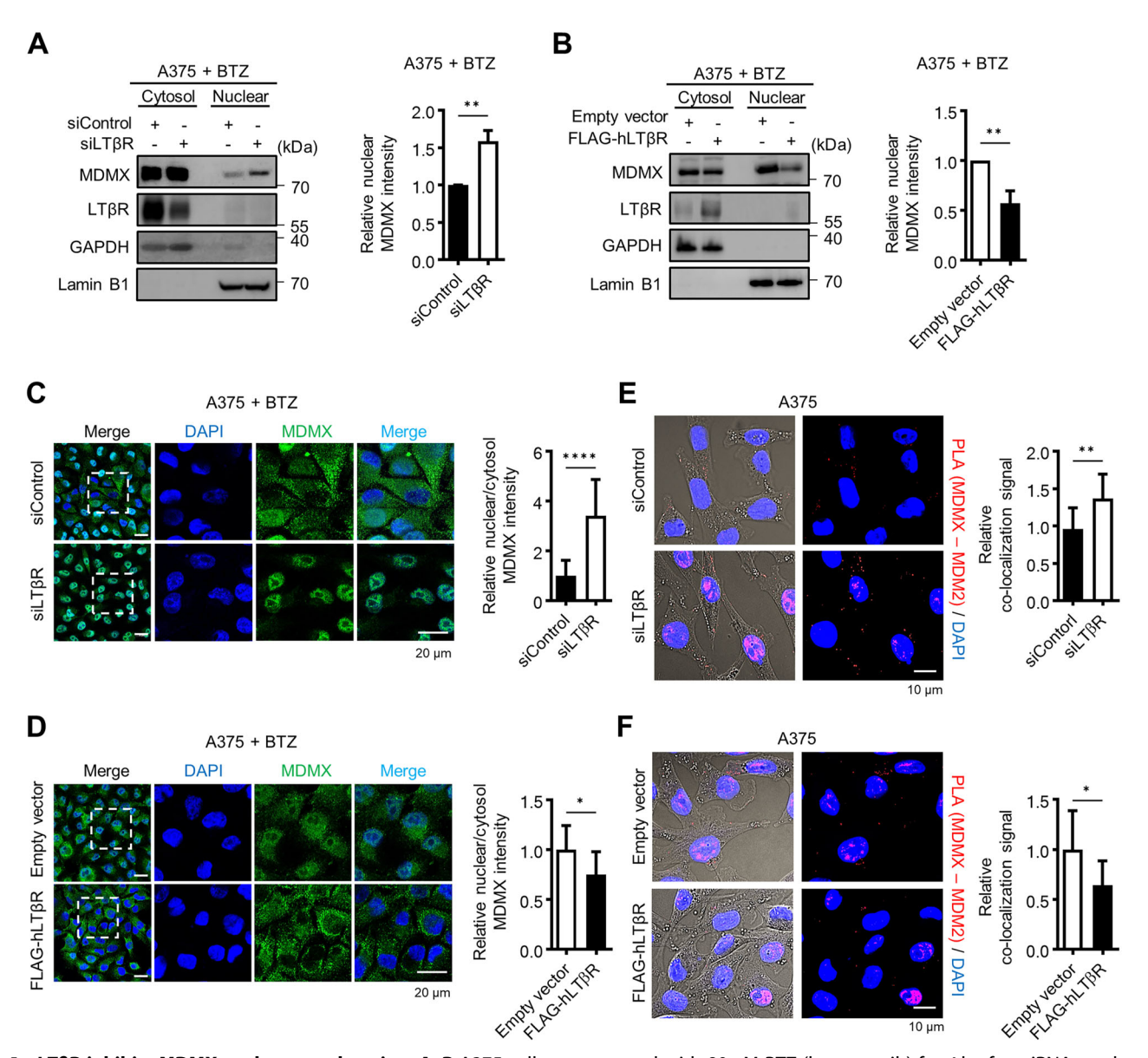


Fig. 5 LTβR inhibits MDMX nuclear translocation. A, B A375 cells were treated with 80 nM BTZ (bortezomib) for 4 h after siRNA or plasmid transfection. Nuclear and cytosol fractions were isolated, followed by western blotting. GAPDH (cytosol) and Lamin B1 (nuclear) were used as loading controls. C, D Confocal microscopy was used to assess MDMX localization. Nuclear MDMX band and fluorescence intensities were measured relative to cytosolic MDMX using ImageJ. E, F PLA was performed to confirm the relative interaction between MDM2 and MDMX in LTβR knockdown cells or LTβR-overexpressing cells. Relative co-localization signals of MDM2 and MDMX (shown in graph) were quantified using ImageJ. Graphical data are presented as means \pm SD (n=3) from three independent experiments. *p < 0.05, **p < 0.01, *****p < 0.0001, using an unpaired Student's t-test.

whether LTBR affects nuclear localization of MDMX, we performed cytosolic and nuclear fractionation following proteasome inhibition using bortezomib (BTZ) to prevent proteasome-mediated degradation of MDMX. Western blot analysis showed that nuclear MDMX levels increased in LTBR knockdown cells but decreased in LTβR-overexpressing cells (Fig. 5A, B). Confocal microscopy results were consistent with the western blot data, showing similar patterns of nuclear MDMX localization (Fig. 5C, D). Comparable results were observed in LTBR KO cells that reconstituted with LTBR (Fig. S7A, B). PLA further confirmed that MDM2-MDMX interaction was enhanced in LTBR knockdown cells but reduced in LTβR-overexpressing cells (Fig. 5E, F). To exclude the potential involvement of the MDMX deubiquitinating enzyme USP7 [46], we performed immunoprecipitation using a USP7 antibody. USP7 has been reported to interact with TRAF6, which in turn modulates NFκB signaling [47, 48]. Interestingly, the interaction between USP7

and TRAF6 was enhanced following LTβR overexpression, whereas the interaction between USP7 and MDMX showed no significant change upon either LTβR knockdown or overexpression (Fig. S7C, D). These findings suggest that LTβR knockdown induces the nuclear localization of MDMX, by upregulating its interaction with MDM2, which in turn facilitates MDMX degradation in the nucleus and subsequently suppresses the degradation of p53.

LTBR KO cells delay tumor growth in vivo

To investigate the senescence phenotype of LT β R KO cells in WT mice, which express potential ligands such as LIGHT and LT α 1 β 2, B16F10^{WT} cells were implanted on the right dorsal side, while B16F10^{LT β R-KO} cells were implanted on the left dorsal side of 8-week-old WT C57/BL6 mice. After 9 days, the mice were treated via intraperitoneal injection with either vehicle (PBS) or Dox (4 mg/kg) to induce a robust synergistic effect on tumor senescence, and were

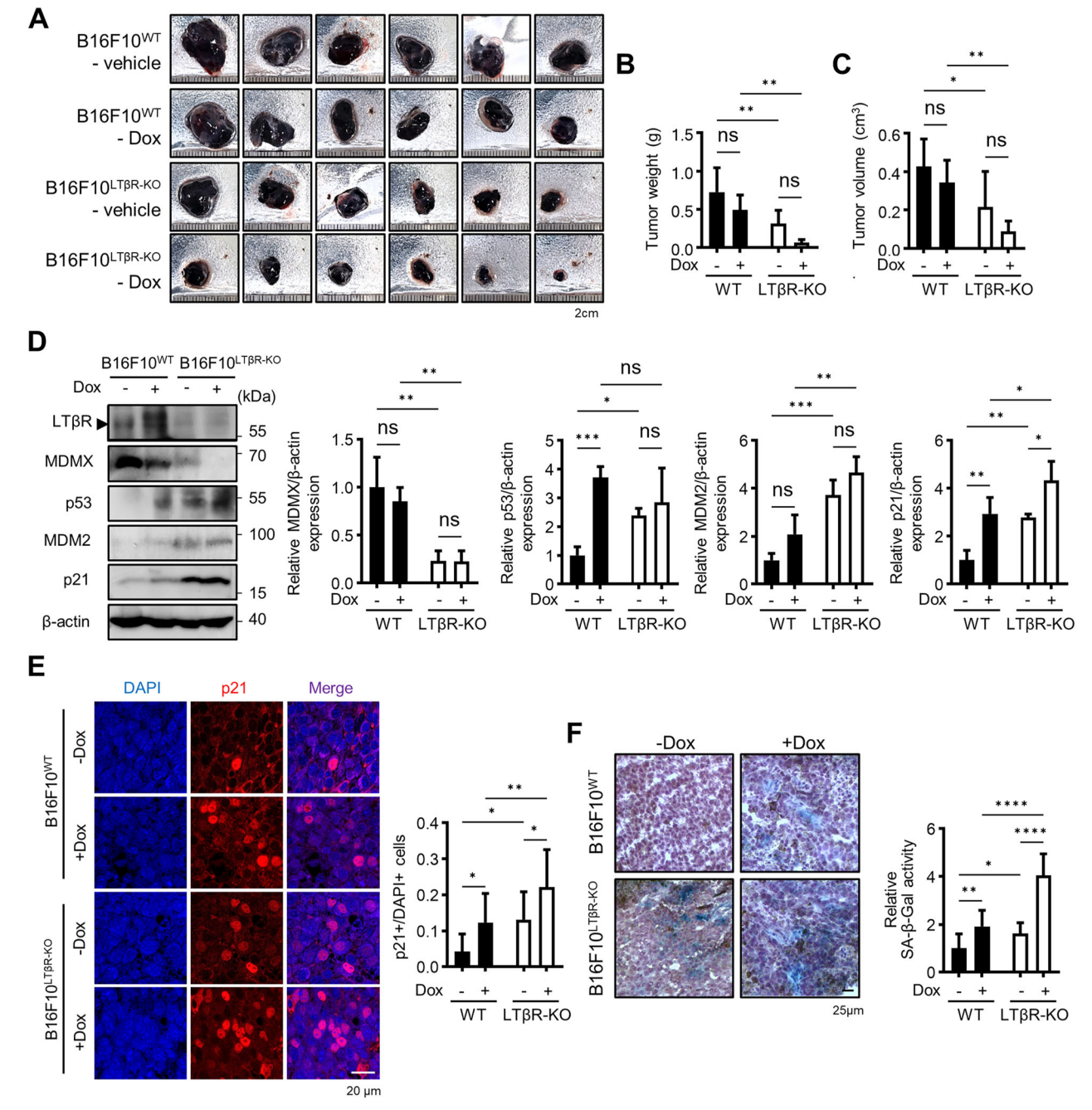


Fig. 6 Depletion of LTβR inhibits tumor growth. Tumors were established by the subcutaneously injecting of B16F10^{WT} and B16F10^{LTβR-KO} cells into mice. On day 9 after implantation, mice were administered with 4 mg Dox per kg of mouse body weight. **A–C** Tumors were harvested on day 16, photographed, and their weight and volume were measured (n = 6). **D** Western blotting of tumor cell lysates for indicated proteins. **E** Paraffin-embedded tissue sections were stained for p21, and relative expression levels were measured using ImageJ. **F** Cryosections of tumor tissue were subjected to SA-β-Gal staining, and relative SA-β-Gal activity was measured using ImageJ. Brown pigments in the histological sections represent melanin deposits. Hematoxylin was used for counterstaining. Graphical data are presented as means \pm SD (n = 3). *p < 0.05, **p < 0.01, ****p < 0.001, *****p < 0.001, *****p < 0.0001, using Fisher's LSD post hoc test. n.s not significant.

sacrificed 7 days later (Fig. 6A). Tumor measurements indicated that B16F10^{LTβR-KO} tumors were significantly smaller in weight and volume compared with B16F10^{WT} tumors (Fig. 6B, C). Western blot analysis of tumor tissues revealed increased levels of p53, MDM2, and p21 in B16F10^{LTβR-KO} tumors (Fig. 6D). Moreover, fluorescent immunohistochemistry confirmed elevated levels of p21, and cryosection analysis showed higher SA- β -Gal activity in B16F10^{LTβR-KO} tumors, highlighting a pronounced senescence phenotype (Fig. 6E, F).

Next, to test the additive effect of MDM2 inhibitor on enhancing p53 activation, mice implanted with B16F10 $^{\rm WT}$ and B16F10 $^{\rm LT\beta R-KO}$ cells were treated with nutlin-3a. As shown in Fig.7A–D, nutlin-3a further supported the role of LT $^{\rm H}$ R in regulating p53-mediated senescence through a decrease in tumor growth. Tumor tissue analysis revealed elevated p21 levels and SA- $^{\rm H}$ Gal staining in nutlin-3a-treated LT $^{\rm H}$ R KO tumors (Fig. 7E, F). These findings indicate that depletion of LT $^{\rm H}$ R delays tumor progression in vivo, suggesting that the combination of LT $^{\rm H}$ R gene targeting and

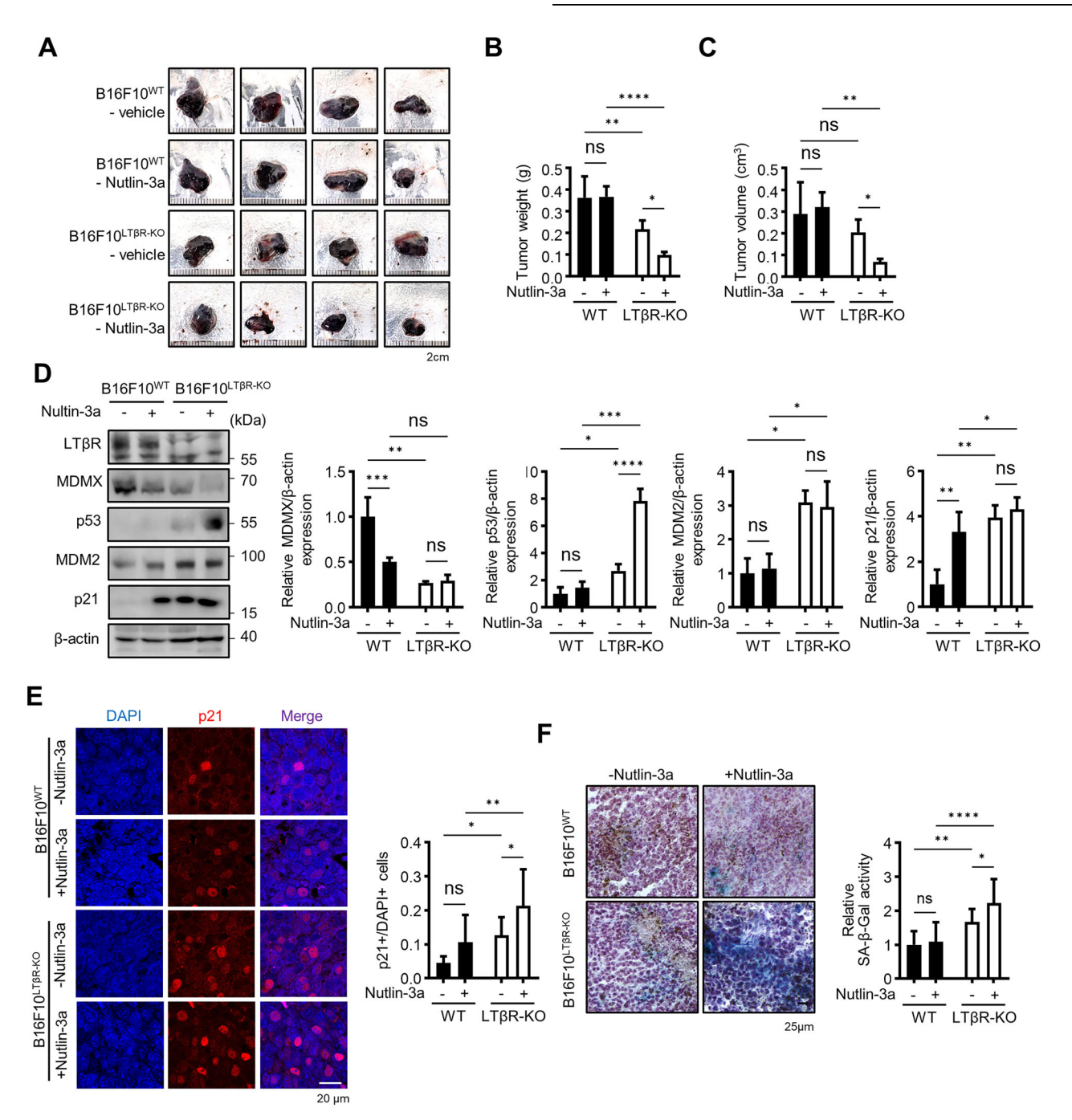


Fig. 7 LTβR depletion synergistically enhances inhibition of tumor growth with nutlin-3a. A–C Tumors were generated by implantating B16F10^{WT} and B16F10^{LTβR-KO} cells into mice. On day 9 after implantation, mice were injected with 20 mg nutlin-3a per kg of mouse body weight. After 7 days, tumors were collected, photographed, and their weight and volume were measured (n = 4). **D** Western blot of tumor cell lysates for indicated proteins. **E** Paraffin-embedded tissue sections were stained for p21, and relative expression was measured. **F** Cryosections of tumor tissue were stained with SA-β-Gal to assess senescence activity. Brown pigments in the histological section indicate melanin deposits. Hematoxylin was used for counterstaining. Graphical data are presented as means ± SD (n = 3). *p < 0.05, **p < 0.01, ****p < 0.001, *****p < 0.0001, using Fisher's LSD post hoc test. n.s not significant.

p53-activating drugs may serve as a potential therapeutic strategy for cancer treatment.

DISCUSSION

LT β R is expressed in various cancer cells, particularly in lung and skin cancers [20]. LT β R stimulation with its ligand LIGHT, or agonist antibodies, as well as overexpression induces apoptosis in cells [17–19, 49]. Despite its known role in inducing apoptosis, the

reason for LT β R overexpression in certain cancers remains poorly understood. To clarify the role of LT β R in cancer cells, LT β R was depleted in melanoma cells using siRNA or the CRISPR/Cas9 system. We observed larger, flattened cells with increased levels of p21 and p53, which are hallmarks of cellular senescence. Conversely, no prominent morphological changes were observed in LT β R-overexpressing cells, but Dox-treated LT β R-overexpressing cells displayed a significant increase in cell number and reduced levels of p53 and p21. Given that p53 mRNA levels remained

unchanged while p21 mRNA levels increased, we investigated MDM2 and MDMX, which are known to regulate p53 degradation.

Unlike MDMX, MDM2 has a nuclear localization signal (NLS), and MDM2 is known to auto-ubiquitinate, but under conditions where MDMX binds to MDM2, MDM2 promotes the degradation of MDMX rather than itself [50]. Recent studies linking MDMX to patient survival [51] imply that therapeutic targeting of MDMX may offer a promising strategy for treating cancers in which MDMX modulates p53 activity [24]. We observed that LTBR expression affects p53 degradation and MDMX stability. We hypothesized that LTBR stabilizes MDMX by inhibiting its interaction with MDM2, thereby preventing MDMX nuclear translocation and subsequent degradation, and this regulation of MDMX in the cytoplasm by LTBR may contribute to p53mediated senescence. In vivo experiments confirmed that LTBR expression affects tumor growth in WT mice, and LTBR knockout tumors exhibited enhanced sensitivity to nutlin-3a, a drug that inhibits MDM2-mediated p53 degradation.

Interestingly, LTBR overexpression induces its self-oligomerization, which leads to its translocation into cells and activation of non-canonical NF-kB signaling [41-44]. This suggests that LTBR-mediated NF-kB signaling can be modulated not only by its ligand binding but also by its own expression. Overexpressing the cytosolic domain of LTβR in HeLa cells, which includes the self-association domain of LTBR, induced cell death [41]. Additionally, LTBR agonist antibodies effectively inhibited tumor growth in colon cancer [10, 17]. Consistent with prior findings, these results suggest LTBR involvement in apoptotic signaling. However, most of the studies indicated that stimulating or overexpressing LTBR induced apoptosis in cells with specific p53 mutations, such as R273H, in the DNA binding domain. For those cells without the p53 mutation, stimulating LTBR has less effect. In this study, we found that knocking down LTBR in HT-29 cells, which also carry the p53 R273H mutation, did not lead to a senescence phenotype, and this suggests that there may be two distinct strategies to target LTBR: blocking it or stimulating it, depending on the p53 status of the cells. We observed that treatment with LIGHT had a paradoxical effect on LTBR, resulting in the downregulation of both p53 and LTBR, while upregulating p21. This study is limited by the absence of experiments involving other ligands and a lack of deeper investigation into the underlying molecular pathways. Therefore, future research should focus on elucidating the molecular interplay between LTβR, NF-κB signaling, and p53 in various cancer types and exploring combination therapies to exploit LTBR-p53 dynamics for improved cancer treatment outcomes. Moreover, studies on inhibitors of LTBR and MDMX, and identifying the precise interaction sites of these molecules are needed to modulate the LTβR-MDMX-p53-p21 axis.

Although we also observed a senescence-like phenotype in other cell lines, we primarily focused on melanoma cell lines to propose a potential cancer-targeting strategy that does not account for immune cell interactions. Additionally, we did not explore gene-targeting strategies in vivo, which may further broaden the therapeutic applicability. Notably, under hypoxic conditions, CREB1 binds to LTBR promoter and regulates its expression [52]. Although LTBR knockdown induces senescence in normal cells such as IMR90, cancer cells are typically exposed to hypoxic environments—where p53 and MDM2 levels are low and LTBR is elevated. In this context, suppressing LTBR levels can serve as a viable strategy. This mechanism may also explain the drug-resistant phenotype observed in patients, further highlighting the potential of targeting LTBR in hypoxic tumors.

In conclusion, our results suggest a potential role for LTβR in regulating p53 by modulating the stability of MDMX, providing insight into its cancer therapeutic strategies.

MATERIALS AND METHODS

Cell culture

Human melanoma A375, mouse melanoma B16F10, and human lung fibroblast IMR90 cell lines were cultured in Dulbecco's Modified Eagle Medium (DMEM, Welgene, Gyeongsan, South Korea). Mouse macrophage J774, human non-small cell lung carcinoma A549, and human colorectal adenocarcinoma HT-29 cell lines were cultured in Roswell Park Memorial Institute (RPMI) medium containing L-Glutamine (Welgene). All media were supplemented with 10% heat-inactivated fetal bovine serum (FBS, Corning, Corning, NY, USA). Cells were incubated at 37 °C and 5% CO₂. Cell lines were purchased from American Type Culture Collection (ATCC) and were confirmed to be free of mycoplasma contamination. For live cell counting, 0.4% trypan blue solution (Gibco, Thermo Fisher Scientific, Waltham, MA, USA) was added to the cell suspension and incubated for 5 min at room. temperature (RT). Viable cells, identified as those without staining, were counted using a hemocytometer under a light microscope. Cellular morphological changes were photographed using an inverted phasecontrast microscope.

Generation of knockout cells

LT β R KO cells were generated using CRISPR/Cas9 KO plasmid system (sc-421483-NIC, Santa Cruz Biotechnology, Dallas, TX, USA) according to the manufacturer's instructions. After 48 h, transfected cells were selected using 2 µg/ml of puromycin (Sigma-Aldrich, St. Louis, MO, USA). GFP-positive cells were then sorted using BD FACS Aria III (BD Biosciences, Franklin Lakes, NJ, USA) and underwent a second round of puromycin selection. To generate monoclonal populations, transfected cells were diluted to 0.5 cells per well and seeded into 96-well plates. Single colonies were expanded in larger culture vessels, and successful LT β R knockout was confirmed using western blotting.

Transfection

Human LTβR (HG10581-NF) and mouse LTβR (MG57382-NM) plasmids were obtained from Sino Biological (Wayne, PA, USA). The LTβR-ΔECD plasmid was synthesized and cloned into the same expression vector as full-form LTBR construct in our laboratory. siRNA duplexes against human and mouse LTBR, human MDMX, and nonspecific control siRNA were purchased from Bioneer Inc. (Daejeon, South Korea). Plasmids and siRNA transfections were performed using Lipofectamine 2000 (Invitrogen, Waltham, MA, USA) and RNAiMAX (Invitrogen), respectively, following the supplier's protocol. After 48 h, cells were subjected to cell counting, SAβ-Gal staining, western blot analysis, real-time PCR, flow cytometry analysis, and immunocytochemistry analysis. For additional experiments, cells were treated with 100 ng/ml doxorubicin (Dox, Cell Signaling Technologies, Danvers, MA, USA), 200 ng/ml recombinant human LIGHT (R&D systems, Minneapolis, MN, USA), and 20 µM nutlin-3a (Selleckchem, Houston, TX, USA) for the indicated time. After transfection, cells were treated with MG-132 (474790, Sigma-Aldrich) for 4 h, and cyclohexamide (CHX, C4859, Sigma-Aldrich) for the designated time.

Western blot analysis

Cells were collected and lysed in RIPA buffer containing protease and phosphatase inhibitors. Nuclear/cytosol fractionation was performed (ab289882, Abcam, Cambridge, UK) according to the manufacturer's protocol. Protein concentrations were quantified using bicinchoninic acid assay. Equal amounts of total protein were resolved via SDS-PAGE and transferred onto nitrocellulose membranes. The membranes were blocked with 5% skim milk or 5% BSA in 0.1% TBS-T. Proteins were detected using the following specific antibodies: α-LTβR (20331-1-AP, Proteintech, Rosemont, IL, USA or PA5-88290, Invitrogen), α-p53 (10442-1-AP, Proteintech), α-p21 (556431, BD Biosciences), α-MDM2 (ab259265, Abcam), α-MDMX (17914-1-AP, Proteintech), α-ΙκΒα (4812S, Cell Signaling Technology, Danvers, MA, USA), α-p52 (4882, Cell Signaling Technology), α-USP7 (66514-1-lg, Proteintech), α-TRAF6 (8028S, Cell Signaling Technology), αlamin B1 (ab16048, Abcam), α-GAPDH (AC002, Abclonal, Wuhan, China), and α-β-actin (sc-47778, Santa Cruz) were used. HRP-conjugated secondary antibodies (Jackson ImmunoResearch, West Grove, PA, USA) were used to detect antigen-antibody complexes, which were further visualized using enhanced chemiluminescent substrate (ECL, GenDEPOT, Barker, TX, USA). The membranes were stripped by submerging them in stripping buffer (Biomax, Rockville, MD, USA) for 20 min under constant shaking at RT.

Confocal microscopy

Cells were cultured in four-well glass slides (SPL Life Sciences, Pocheon, South Korea) and fixed using 4% paraformaldehyde solution. After permeabilization with 0.1% Triton X-100, cells were stained using the specific antibodies, followed by a fluorochrome-tagged secondary antibody. The following antibodies were used: α-MDMX (17914-1-AP, Proteintech), α-p21 (556431, BD Biosciences), and α-Ki67 (ab15580, Abcam). Slides were mounted using Fluoromount-G™ Mounting Medium, with DAPI (Invitrogen) and observed under confocal microscopy (ZEISS, LSM700, Jena, Germany). To quantify nuclear MDMX fluorescence intensity relative to cytosolic MDMX, we analyzed green fluorescence images using ImageJ. Nuclear regions were identified by overlaying the DAPI-stained image, and these nuclear regions were excluded to isolate the cytosolic signal. The fluorescence intensity was measured separately in the cytoplasmic and nuclear compartments. To normalize the data, the total intensity was divided by the number of nuclei (determined by DAPIpositive cells).

Real-time PCR

Total RNA was extracted 48 h post-transfection using AccuPrep® Universal RNA Extraction Kit (Bioneer, Daejeon, South Korea) following the manufacturer's protocol. Oligo (dT) primer was used to generate 2 μg of cDNA in premix (Takara Bio Inc., Shiga, Japan). Real-time PCR was performed using the Power SYBR™ Green PCR Master Mix (Thermo Scientific), as per the manufacturer's instructions. Relative quantification of mRNA expression levels was calculated using the 2^{-ΔΔCt} method. All real-time PCR reactions were performed in triplicate.

Immunoprecipitation

Interaction between LTßR and MDMX was confirmed by immunoprecipitation. Cells were lysed using RIPA buffer and centrifuged at 4 °C, 15,000 rpm for 40 min. DynabeadsTM Protein G (Invitrogen) were pre-incubated with ~1–2 µg of MDMX antibody (17914-1-AP, Proteintech), LTßR antibody (16-5671-82, Invitrogen), α-USP7 (66514-1-Ig, Invitrogen), Flag antibody (F7425, Sigma-Aldrich), or IgG (12-371, Sigma-Aldrich) for 1 h at RT. The antibody-coated beads were further incubated with cell lysate. After 3 washes with lysis buffer, the bound proteins were eluted by boiling the beads at 100 °C for 7 min. For immunoprecipitation of ubiquitinated protein, cells with bortezomib (BTZ, 50 nM) for 4 h, and N-ethylmaleimide (NEM, 10 mM) was added in the lysis buffer. After centrifugation of lysate, residual NEM in the supernatants was neutralized by adding dithiothreitol (DTT) to a final concentration of 10 mM, as previously described [53].

Proximity ligation assay (PLA)

PLA was performed after 48 h of LTβR siRNA or plasmid transfection in both A375 and B16F10 cells. Cells were cultured in 8-well Nunc™ Lab-Tek™ Chamber Slide System (Thermo Scientific) and fixed using 4% paraformal-dehyde for 10 min at RT. Following permeabilization with 0.1% Triton X-100, the Duolink® Proximity Ligation Assay (Sigma-Aldrich) was performed according to the manufacturer's protocol. A375 cells were incubated with antibodies to LTβR (20331-1-AP, Proteintech), MDMX (sc-374147, Santa Cruz), and MDM2 (ab259265, Abcam). While B16F10 cells were incubated with antibodies to LTβR (16-5671-82, Invitrogen) and MDMX (17914-1-AP, Proteintech).

SA-B-Gal staining

To evaluate cellular SA-β-Gal activity, SA-β-Gal staining was performed on day 2 post-treatment using β-Galactosidase staining solution (pH 6.0, 5 mM potassium ferrocyanide, 5 mM potassium ferricyanide, 40 mM citric acid/ sodium phosphate, 150 mM NaCl, 2 mM MgCl₂, and 1 mg/ml X-Gal) or CellEvent™ Senescence Green Detection Kit (Invitrogen). Cellular morphological changes were photographed using an inverted phase-contrast microscope (Olympus, Tokyo, Japan). For tissue SA-β-Gal staining, excised tumors were washed with PBS and embedded in an O.C.T. Compound (Leica Biosystems, Buffalo Grove, IL, USA). Frozen tissues were sectioned into 20 µm-thick slices using a cryostat (Leica Biosystems). Cryosections were washed with 1x PBS, fixed with 0.2% glutaraldehyde for 10 min, RT, and stained with a β-Galactosidase staining solution. Sections were incubated at 37 $^{\circ}\text{C}$ for 12–16 h. After washing twice with PBS, sections were stained with hematoxylin for nuclear visualization and covered with a cover glass using a Fluoromount-G™ Mounting Medium (Invitrogen). Images were obtained using an inverted phase-contrast microscope [54].

Mouse experiment

All animal procedures were approved by the Institutional Animal Care and Use Committee (IACUC no. 2023-0146). Briefly, 8-week-old female BALB/c mice were housed in a specific pathogen-free facility and were used for allograft tumor experiments. Mice were randomly assigned, but the experiments were not blinded. To generate tumors, 1×10^6 B16F10 $^{\rm WT}$ and B16F10 $^{\rm LTBR-KO}$ cells were suspended in 100 μ l PBS, injected into the dorsal subcutaneous area of mice, and successfully formed tumor masses after implantation. Mice were administered a single intraperitoneal injection of doxorubicin (4 mg/kg body weight) or nutlin-3a (20 mg/kg body weight) after tumor formation, and tumors were collected after 7 days. Tumor tissues were fixed overnight in 4% formalin and embedded in paraffin. These sections were prepared for immunohistochemistry to detect p21 and MDMX. Subsequently, the slices were counterstained with DAPI. Images were captured from randomly selected areas of each tumor section, following standard protocols.

Statistical analysis

Statistical analysis and data visualization were conducted using GraphPad Prism 10 software (GraphPad Software, San Diego, CA, USA). For comparisons between two groups, statistical significance was determined by unpaired t-test or multiple unpaired t-tests with false discovery rate (FDR) correction, using a threshold of FDR < 0.01. For comparisons involving two independent variables, two-way ANOVA was performed, followed by uncorrected Fisher's least significant difference (LSD) test, Tukey's multiple comparison test, or Šidák's multiple comparison test. Each experiment was independently performed at least three times, with similar results.

DATA AVAILABILITY

Original data are available upon request. The full length, uncropped original western blots are shown in the 'Supplementary Material'.

REFERENCES

- Mikami Y, Matsuzaki H, Horie M, Noguchi S, Jo T, Narumoto O, et al. Lymphotoxin β receptor signaling induces IL-8 production in human bronchial epithelial cells. PLoS ONE. 2014:9:e114791.
- Shou YJ, Koroleva E, Spencer CMM, Shein SAA, Korchagina AAA, Yusoof KAA, et al. Redefining the role of lymphotoxin beta receptor in the maintenance of lymphoid organs and immune cell homeostasis in adulthood. Front Immunol. 2021;12:712632.
- Tamada K, Shimozaki K, Chapoval AI, Zhai Y, Su J, Chen SF, et al. LIGHT, a TNF-like molecule, costimulates T cell proliferation and is required for dendritic cellmediated allogeneic T cell response. J Immunol. 2000;164:4105–10.
- Chin RK, Zhu M, Christiansen PA, Liu W, Ware C, Peltonen L, et al. Lymphotoxin pathway-directed, autoimmune regulator-independent central tolerance to arthritogenic collagen. J Immunol. 2006;177:290–7.
- Wimmer N, Huber B, Barabas N, Röhrl J, Pfeffer K, Hehlgans T. Lymphotoxin β
 receptor activation on macrophages induces cross-tolerance to TLR4 and TLR9
 ligands. J Immunol. 2012;188:3426–33.
- Wimmer N, Heigl U, Klingseisen L, Schneider-Brachert W, Hehlgans T. Lymphotoxin-beta receptor signalling regulates cytokine expression via TRIM30α in a TRAF3-dependent manner. Mol Immunol. 2013;54:40–7.
- Futterer A, Mink K, Luz A, Kosco-Vilbois MH, Pfeffer K. The lymphotoxin beta receptor controls organogenesis and affinity maturation in peripheral lymphoid tissues. Immunity. 1998;9:59–70.
- 8. Kwok, Medovich T, Silva SC, IJr, Brown EM, Haug JC, et al. Age-associated changes to lymph node fibroblastic reticular cells. Front Aging. 2022;3:838943.
- Wolf MJ, Seleznik GM, Zeller N, Heikenwalder M. The unexpected role of lymphotoxin beta receptor signaling in carcinogenesis: from lymphoid tissue formation to liver and prostate cancer development. Oncogene. 2010;29:5006–18.
- Hu XL, Zimmerman MA, Bardhan K, Yang DF, Waller JL, Liles GB, et al. Lymphotoxin β receptor mediates caspase-dependent tumor cell apoptosis and tumor suppression despite induction of NF-κB activation. Carcinogenesis. 2013;34:1105–14.
- Kuai J, Nickbarg E, Wooters J, Qiu YC, Wang J, Lin LL. Endogenous association of TRAF2, TRAF3, cIAP1, and Smac with lymphotoxin β receptor reveals a novel mechanism of apoptosis. J Biol Chem. 2003;278:14363–9.
- Dejardin E, Droin NM, Delhase M, Haas E, Cao Y, Makris C, et al. The lymphotoxinbeta receptor induces different patterns of gene expression via two NF-κB pathways. Immunity. 2002;17:525–35.

- Rooney IA, Butrovich KD, Glass AA, Borboroglu S, Benedict CA, Whitbeck JC, et al. The lymphotoxin-β receptor is necessary and sufficient for LIGHT-mediated apoptosis of tumor cells. J Biol Chem. 2000;275:14307–15.
- Conlon TM, John-Schuster G, Heide D, Pfister D, Lehmann M, Hu Y, et al. Inhibition of LTβR signalling activates WNT-induced regeneration in lung. Nature. 2020:588:151–6.
- Heo S, Noh E, Kim J, Jo J, Choi Y, Kim H. LIGHT (TNFSF14) increases the survival and proliferation of human bone marrow-derived mesenchymal stem cells. PLoS ONE. 2016;11:e0166589.
- Kotov JA, Xu Y, Carey ND, Cyster JG. LTβR overexpression promotes plasma cell accumulation. PLoS ONE. 2022;17:e0270907.
- Lukashev M, LePage D, Wilson C, Bailly V, Garber E, Lukashin A, et al. Targeting the lymphotoxin-β receptor with agonist antibodies as a potential cancer therapy. Cancer Res. 2006;66:9617–24.
- Haybaeck J, Zeller N, Wolf MJ, Wagner U, Kurrer MO, Bremer J, et al. A lymphotoxin-driven pathway to hepatocellular carcinoma. Cancer Cell. 2009:16:295–308.
- Tang HD, Wang Y, Chlewicki LK, Zhang Y, Guo JY, Liang W, et al. Facilitating T cell infiltration in tumor microenvironment overcomes resistance to PD-L1 blockade. Cancer Cell. 2016;30:500.
- Wu YT, Zhao SJ, Guo WL, Liu Y, Mullor MDR, Rodriguez RA, et al. Systematic analysis of the prognostic value and immunological function of LTBR in human cancer. Aging. 2024;16:129–52.
- Fujiwara S, Yamashita Y, Choi YM, Wada T, Kaneda R, Takada S, et al. Transforming activity of the lymphotoxin-β receptor revealed by expression screening. Biochem Biophys Res Commun. 2005;338:1256–62.
- Chen JD. The cell-cycle arrest and apoptotic functions of p53 in tumor initiation and progression. Csh Perspect Med. 2016;6:a026104.
- Linares LK, Hengstermann A, Ciechanover A, Muller S, Scheffner M. HdmX stimulates Hdm2-mediated ubiquitination and degradation of p53. Proc Natl Acad Sci USA. 2003;100:12009–14.
- Migliorini D, Danovi D, Colombo E, Carbone R, Pelicci PG, Marine JC. Hdmx recruitment into the nucleus by Hdm2 is essential for its ability to regulate p53 stability and transactivation. J Biol Chem. 2002;277:7318–23.
- LeBron C, Chen LH, Gilkes DM, Chen JD. Regulation of MDMX nuclear import and degradation by Chk2 and 14-3-3. EMBO J. 2006;25:1196–206.
- 26. Feng ZH, Hu WW, Rajagopal G, Levine AJ. The tumor suppressor p53 cancer and aging. Cell Cycle. 2008;7:842–7.
- 27. Mijit M, Caracciolo V, Melillo A, Amicarelli F, Giordano A. Role of p53 in the regulation of cellular senescence. Biomolecules. 2020;10:420.
- Di Micco R, Krizhanovsky V, Baker D, di Fagagna FD. Cellular senescence in ageing: from mechanisms to therapeutic opportunities. Nat Rev Mol Cell Biol. 2021;22:75–95.
- Hernandez-Segura A, Nehme J, Demaria M. Hallmarks of cellular senescence. Trends Cell Biol. 2018:28:436–53.
- Herranz N, Gil J. Mechanisms and functions of cellular senescence. J Clin Investig. 2018;128:1238–46.
- Kumari R, Jat P. Mechanisms of cellular senescence: cell cycle arrest and senescence associated secretory phenotype. Front Cell Dev Biol. 2021;9:645593.
- Childs BG, Baker DJ, Kirkland JL, Campisi J, van Deursen JM. Senescence and apoptosis: dueling or complementary cell fates?. EMBO Rep. 2014;15:1139–53.
- Fitsiou E, Soto-Gamez A, Demaria M. Biological functions of therapy-induced senescence in cancer. Semin Cancer Biol. 2022;81:5–13.
- 34. Beck J, Turnquist C, Horikawa I, Harris C. Targeting cellular senescence in cancer and aging: roles of p53 and its isoforms. Carcinogenesis. 2020;41:1017–29.
- Sturmlechner I, Sine CC, Jeganathan KB, Zhang C, Velasco ROF, Baker DJ, et al. Senescent cells limit p53 activity via multiple mechanisms to remain viable. Nat Commun. 2022;13:3722.
- 36. Höpner SS, Raykova A, Radpour R, Amrein MA, Koller D, Baerlocher GM, et al. LIGHT/LTβR signaling regulates self-renewal and differentiation of hematopoietic and leukemia stem cells. Nat Commun. 2021;12:1065.
- Hu BL, Gilkes DM, Farooqi B, Sebti SM, Chen JD. MDMX overexpression prevents p53 activation by the MDM2 inhibitor nutlin. J Biol Chem. 2006;281:33030–5.
- Wiley CD, Schaum N, Alimirah F, Lopez-Dominguez JA, Orjalo AV, Scott G, et al. Small-molecule MDM2 antagonists attenuate the senescence-associated secretory phenotype. Sci Rep. 2018;8:2410.
- Honorato RV, Trellet ME, Jimenez-Garcia B, Schaarschmidt JJ, Giulini M, Reys V, et al. The HADDOCK2.4 web server for integrative modeling of biomolecular complexes. Nat Protoc. 2024;19:3219–41.
- Honorato RV, Koukos PI, Jimenez-Garcia B, Tsaregorodtsev A, Verlato M, Giachetti A, et al. Structural Biology in the Clouds: The WeNMR-EOSC Ecosystem. Front Mol Biosci. 2021;8:729513.
- 41. Wu MY, Wang PY, Han SH, Hsieh SL. The cytoplasmic domain of the lymphotoxin- β receptor mediates cell death in HeLa cells. J Biol Chem. 1999;274:11868–73.

- 42. Force WR, Glass AA, Benedict CA, Cheung TC, Lama J, Ware CF. Discrete signaling regions in the lymphotoxin-beta receptor for tumor necrosis factor receptor-associated factor binding, subcellular localization, and activation of cell death and NF-κB pathways. J Biol Chem. 2000;275:11121–9.
- 43. Remouchamps C, Boutaffala L, Ganeff C, Dejardin E. Biology and signal transduction pathways of the Lymphotoxin- $\alpha\beta$ /LT β R system. Cytokine Growth Factor Rev. 2011;22:301–10.
- Maksymowicz M, Miaczynska M, Banach-Orlowska M. Clathrin- and dynamindependent endocytosis limits canonical NF-κB signaling triggered by lymphotoxin β receptor. Cell Commun. Signal. 2020;18:176.
- Gu JJ, Kawai H, Nie LG, Kitao H, Wiederschain D, Jochemsen AG, et al. Mutual dependence of MDM2 and MDMX in their functional inactivation of p53. J Biol Chem. 2002;277:19251–4.
- Qi SM, Cheng G, Cheng XD, Xu Z, Xu B, Zhang WD, et al. Targeting USP7mediated deubiquitination of MDM2/MDMX-p53 pathway for cancer therapy: are we there yet?. Front Cell Dev Biol. 2020;8:233.
- 47. Xiang Q, Ju H, Nicholas J. USP7-dependent regulation of TRAF activation and signaling by a viral interferon regulatory factor homologue. J Virol. 2020;94. https://doi.org/10.1128/JVI.01553-19.
- Abe T, Barber GN. Cytosolic-DNA-mediated, STING-dependent proinflammatory gene induction necessitates canonical NF-kappaB activation through TBK1. J Virol. 2014;88:5328–41.
- Scarzello AJ, Jiang Q, Back T, Dang H, Hodge D, Hanson C, et al. LTβR signalling preferentially accelerates oncogenic AKT-initiated liver tumours. Gut. 2016:65:1765–75.
- Linke K, Mace PD, Smith CA, Vaux DL, Silke J, Day CL. Structure of the MDM2/ MDMX RING domain heterodimer reveals dimerization is required for their ubiquitylation in trans. Cell Death Differ. 2008;15:841–8.
- Liu J, Yang J, Pan QL, Wang XY, Wang XY, Chen H, et al. MDM4 was associated with poor prognosis and tumor-immune infiltration of cancers. Eur J Med Res. 2024;29:79.
- Hu ZY, Zhou GP. CREB1 transcriptionally activates LTBR to promote the NF-κB Pathway and apoptosis in lung epithelial cells. Comput. Math Methods Med. 2022:2022:9588740.
- Sparks A, Dayal S, Das J, Robertson P, Menendez S, Saville MK. The degradation of p53 and its major E3 ligase Mdm2 is differentially dependent on the proteasomal ubiquitin receptor S5a. Oncogene. 2014;33:4685–96.
- Jannone G, Rozzi M, Najimi M, Decottignies A, Sokal EM. An optimized protocol for histochemical detection of senescence-associated beta-galactosidase activity in cryopreserved liver tissue. J Histochem Cytochem. 2020;68:269–78.

AUTHOR CONTRIBUTIONS

S.Y.K., J.-J.L., and J.-S.S. contributed to conception and design. S.Y.K. performed experiments, analyzed and interpreted the data, and drafted the manuscript. B.L. contributed to experiments related to animal study and protein stability. W.J.R. contributed to experiments related to protein binding. B.L., J.-J.L., M.S.K., W.J.R., I.H.P., and J.-S.S. contributed to writing the manuscript. J.-S.S. supervised all aspects of the study and handled funding.

FUNDING

This study was supported by grants from the National Research Foundation of Korea (NRF), funded by the Korean government [RS-2019-NR040072 and RS-2022-NR068972] and the Research Center Program of the Institute for Basic Science (IBS) in Korea (IBS-R026-D1).

COMPETING INTERESTS

The authors declare no competing interests.

ETHICS APPROVAL

All animal procedures were approved by the Institutional Animal Care and Use Committee (IACUC) of Yonsei University College of Medicine (IACUC no. 2023-0146) and were performed in accordance with the Guide for the Care and Use of Laboratory Animals (National Research Council).

ADDITIONAL INFORMATION

Supplementary information The online version contains supplementary material available at https://doi.org/10.1038/s41420-025-02708-1.

Correspondence and requests for materials should be addressed to Jeon-Soo Shin.

Reprints and permission information is available at http://www.nature.com/reprints

Publisher's note Springer Nature remains neutral with regard to jurisdictional claims in published maps and institutional affiliations.

Open Access This article is licensed under a Creative Commons Attribution 4.0 International License, which permits use, sharing, adaptation, distribution and reproduction in any medium or format, as long as you give appropriate credit to the original author(s) and the source, provide a link to the Creative Commons licence, and indicate if changes were made. The images or other third party material in this article are included in the article's Creative Commons licence, unless indicated otherwise in a credit line to the material. If material is not included in the article's Creative Commons licence and your intended use is not permitted by statutory regulation or exceeds the permitted use, you will need to obtain permission directly from the copyright holder. To view a copy of this licence, visit http://creativecommons.org/licenses/by/4.0/.

© The Author(s) 2025